ISSN 1063-7761, Journal of Experimental and Theoretical Physics, 2020, Vol. 130, No. 3, pp. 358–369. © Pleiades Publishing, Inc., 2020.
Russian Text © The Author(s), 2020, published in Zhurnal Eksperimental'noi i Teoreticheskoi Fiziki, 2020, Vol. 157, No. 3, pp. 428–441.

ATOMS, MOLECULES, OPTICS

Fine Structure of the Crossing Resonance Spectrum of Wavefields in an Inhomogeneous Medium

V. A. Ignatchenko[a],* and D. S. Polukhin[a],**

[a] *Kirensky Institute of Physics, Federal Research Center "Krasnoyarsk Science Center," Siberian Branch, Russian Academy of Sciences, Krasnoyarsk, 660036 Russia*

** e-mail: vignatch@iph.krasn.ru*

*** e-mail: polukhin@iph.krasn.ru*

Received June 30, 2019; revised August 9, 2019; accepted August 15, 2019

Abstract—The crossing resonance of two wavefields $m(x, t)$ and $u(x, t)$ of different natures in an inhomogeneous medium with zero mean value of the coupling parameter η between fields has been studied. The stages of formation of the fine structure of the crossing resonance have been analyzed. It has been shown within the model of independent crystallites that the removal of the degeneracy of eigenfrequencies of these fields at the crossing resonance point has a threshold character in the coupling parameter and occurs under the condition $\eta > \eta_c$, where $\eta_c = |\Gamma_u - \Gamma_m|/2$, Γ_u and Γ_m are the relaxation parameters of the corresponding wavefields. At $\eta > \eta_c$, each random implementation of the Green's functions $\tilde{G}''_{mm}$ and $\tilde{G}''_{uu}$ of wavefields has the form of two resonance peaks with the same half-width $(\Gamma_u + \Gamma_m)/2$ spaced by the interval 2η; this form is standard for crossing resonances. At $\eta < \eta_c$, the functions $\tilde{G}''_{mm}$ and $\tilde{G}''_{uu}$ are different: if $\Gamma_u > \Gamma_m$, the function $\tilde{G}''_{mm}$ has the form of a narrow resonance peak at $\omega = \omega_r$, whereas the function $\tilde{G}''_{uu}$ has the form of a broader resonance peak split at the top by a narrow antiresonance. Averaging over regions where $\eta > \eta_c$ leads to the formation of a broad resonance with a resonance line half-width of about $\langle\eta^2\rangle^{1/2}$ on the both averaged Green's functions, which is due to the stochastic distribution of resonance frequencies. Averaging over regions where $\eta < \eta_c$ results in the sharpening of a resonance peak on the function G''_{mm} and an antiresonance peak on the function G''_{uu} at the same frequency $\omega = \omega_r$. As a result, a pattern of the crossing resonance in the inhomogeneous medium is formed, consisting of identical broad peaks on both functions with the narrow resonance peak of the fine structure on the function G''_{mm} and the antiresonance peak on the function G''_{uu}. Thus, the fine structure of the spectrum of any crossing resonance of two wavefields of different natures in the inhomogeneous medium is due to the contribution of random realizations corresponding to degenerate states of the natural oscillations of the system. In a ferromagnet with a spatially inhomogeneous coupling parameter, spin and elastic waves acquire damping parameters $\Gamma_m(k) \propto k_c v_m$ and $\Gamma_u(k) \propto k_c v_u$ proportional to the correlation wavenumber k_c of inhomogeneities and to the velocities of the corresponding waves, which are summed with the homogeneous damping parameters Γ_m and Γ_u of the same waves. This situation has been considered in a new self-consisting approximation for the case where the contribution of homogeneous damping parameters is negligibly small. It has been shown that the form of the fine structure on the functions G''_{mm} and G''_{uu} at the second (high-frequency) crossing point of dispersion curves of spin and elastic waves changes to the opposite form: narrow resonance peaks of the fine structure appear on the function G''_{uu}, and antiresonance peaks arise on the function G''_{mm} because $v_m < v_u$ and $v_m > v_u$ at the first and second crossing points, respectively.

DOI: 10.1134/S1063776120010033

1. INTRODUCTION

Magnetoelastic (magnetoacoustic) resonance, which is one of the types of crossing resonance of two interacting wavefields of different physical natures, in a homogeneous medium was studied in [1–9] both theoretically and experimentally. Near the crossing resonance occurring at the crossing of dispersion curves of two interacting wavefields, the degeneracy of eigenfrequencies of a system is lifted, a shift appears between energy levels, and two resonance peaks arise on the frequency dependences of the imaginary parts of Green's functions, the distance between which is determined by the coupling parameter ε between wavefields.

The first studies of the crossing resonance in a medium with the inhomogeneous coupling parameter $\varepsilon(\mathbf{x})$, where $\mathbf{x} = \{x, y, z\}$ [10–13], performed in the Bourret approximation [14] (single scattering of waves by inhomogeneities of the coupling parameter) predicted the existence of disorder-stimulated crossing resonance in the medium with zero mean value of the coupling parameter. However, the adequate description of this phenomenon in the mentioned approximation was impossible because it requires the inclusion of multiple scattering of waves by inhomogeneities of the coupling parameter.

To take into account multiple scattering, we used in [15–18] the self-consistent approximation (SCA) [19–22], which is widely applied to approximately calculate Green's functions. This approximation in different fields of physics has different names (Migdal, Kraichnan, and Born approximations); for this reason, in the cited and subsequent works, we first referred to this approximation as the approximation of nonoverlapping correlations and, then, as the standard self-consistent approximation. The standard SCA involves only diagrams with noncrossing correlation/interaction lines, because it is derived with the inclusion of only the first term of the expansion of the vortex function (i.e., the vortex function is taken to be unity).

The standard SCA was generalized to the case of two interacting wavefields of different physical natures with a stochastically inhomogeneous coupling parameter between these fields whose mean value is zero. Using the developed method, we studied disorder-induced crossing resonance occurring at the crossing of dispersion curves of spin and elastic waves. The inclusion of multiple scattering of waves by inhomogeneities led to the results significantly different from those previously obtained for such a situation in the Bourret approximation in [10–13]. Instead of the removal of degeneracy of frequencies in the spectrum of waves and splitting of resonance peaks of dynamic susceptibilities, each of the imaginary parts G_m'' and G_u'' of the Green's functions of the elastic and spin waves, respectively, should have a broad single-mode peak at the crossing point of unperturbed dispersion curves. The fine structure in the form of narrow resonance and antiresonance peaks appears on the top of this peak in the imaginary parts G_m'' and G_u'' of the Green's functions, respectively. It was shown that the widths of broad peaks at a low correlation wavenumber k_c ($k_c = r_c^{-1}$, where r_c is the correlation radius of inhomogeneities of the coupling parameter $\varepsilon(\mathbf{x})$), are determined by the rms fluctuation of the coupling parameter $\Delta\varepsilon$, whereas the widths of the narrow resonance and antiresonance peaks are determined by the correlation wavenumber k_c. This allows measuring both these main characteristics of inhomogeneities independently. An increase in k_c is accompanied by the sharp exchange-induced narrowing of the broad peak and by the broadening of narrow resonance and antiresonance peaks, which results in the gradual disappearance of these narrow peaks. We also studied the situation where the rms fluctuation $\Delta\varepsilon$ and mean value ε of the coupling parameter are nonzero [17, 18].

The standard SCA allowed studying the main features of the crossing resonance in the inhomogeneous medium. At the same time, disadvantages of this approach were manifested. The well-known demerit of the approach is a dome-like shape of resonance curves, which results in a number of defects at approaching crossing resonance peaks: bends appear on the slopes of the peaks in the imaginary parts of the Green's functions, a false central peak arises, which is not related to the fine structure, etc. These defects could sometimes provide doubts in some conclusions of our previous works; therefore, the next improvement of this approximation became necessary. The authors of [23–32] developed various approaches to the inclusion of vortex corrections to the self-energy or to the Green's function, but discrepancy between the results obtained within various approaches remains very significant although a great advance was achieved. For the case of one wavefield, we derived in [33] a new SCA including both the first and second terms of the expansion of the vortex function.

The standard SCA and Bourret (Born) approximation are limiting cases of the new SCA. In [34], we compared the new SCA to various existing approximations and to the numerical simulation of the solution of the wave equation for a medium with one-dimensional inhomogeneities. We showed that the new SCA has obvious advantages in application to media with long-wavelength inhomogeneities because it describes the shape, width, and height of peaks much better than the standard SCA. The developed mathematical method based on the new SCA was used in [35] to analyze the magnetoelastic resonance in the medium with a partially or completely stochastized coupling parameter. The method is applicable in a wide range of the correlation wavenumber of inhomogeneities k_c from $k_c = 0$ (infinite correlation radius) to k_c values corresponding to the classical limit.

The main result provided by the new method is a significant improvement of the shape of resonance peaks of the dynamic susceptibility, which corrected all defects obtained in [15–18]. The new SCA qualitatively reproduces the previous standard SCA results on the broadening and approach of magnetoelastic resonance peaks and their merging to a single broad peak with an increase in the rms fluctuation $\Delta\varepsilon$ and a decrease in the mean value ε of the coupling parameter. Most importantly, the appearance of the fine structure of the spectrum in the form of a narrow resonance peak on the Green's function of spin waves and a narrow dip (antiresonance) on the Green's function of elastic waves was confirmed. This effect

should be manifested at the interaction of any wave-fields of different physical natures. A hypothesis of the origin of the fine structure was discussed in [15–18]. However, this problem was not exactly solved because of the complex mathematical technique of the theory and the necessity of using numerical methods to obtain particular results.

The aim of this work is to explain the nature of the fine structure of the crossing resonance spectrum. To this end, we consider the magnetoelastic resonance at both crossing points of dispersion curves of spin and elastic waves (Section 2) and the crossing resonance within the model of an inhomogeneous medium with the infinite correlation radius (Section 3).

2. MAGNETOELASTIC RESONANCE AT BOTH CROSSING POINTS OF DISPERSION CURVES

2.1. System of Equations of Matrix Green's Functions

As in [15–18], we consider a coupled system of two scalar equations for the resonance circular projections of the magnetization m and elastic displacements u, where only the dimensionless magnetoelastic coupling parameter $\varepsilon(\mathbf{x})$ is inhomogeneous, where $\mathbf{x} = \{x, y, z\}$:

$$\alpha(\nabla^2 + \nu_m)m - \varepsilon(\mathbf{x})M\frac{\partial u}{\partial z} = -h, \tag{1}$$

$$\mu(\nabla^2 + \nu_u)u + M\frac{\partial}{\partial z}(\varepsilon(\mathbf{x})m) = -f. \tag{2}$$

Here, α is the exchange parameter, μ is the elastic force constant, M is the static magnetization along the external d.c. magnetic field $\mathbf{H}$ (the amplitude of transverse circular projections is $m \ll M$), $\mathbf{h}$ is the external a.c. magnetic field perpendicular to the field $\mathbf{H}$, f is the external mass force, and

$$\nu_m = \frac{\omega - \omega_0}{\alpha g M}, \quad \nu_u = \frac{\omega^2}{v_u^2}. \tag{3}$$

Here, g is the gyromagnetic ratio, ω is the frequency, ω_0 is the frequency of the uniform ferromagnetic resonance depending on the magnetic field H and demagnetizing factors of the sample, and $v_u = \sqrt{\mu/p}$ is the velocity of the elastic wave, where p is the density of the medium.

We represent the magnetoelastic parameter $\varepsilon(\mathbf{x})$ in the form

$$\varepsilon(\mathbf{x}) = \varepsilon + \Delta\varepsilon\rho(\mathbf{x}), \tag{4}$$

where ε is the mean value of this parameter, $\Delta\varepsilon$ is its rms fluctuation, and $\rho(\mathbf{x})$ is a centered ($\rho(\mathbf{x}) = 0$) normalized ($\langle\rho^2(\mathbf{x})\rangle = 1$) random function of the coordinates. Angle brackets mean the average over the ensemble of realizations of this random function.

The stochastic properties of inhomogeneities $\rho(\mathbf{x})$ are characterized by a correlation function K depending on the difference of coordinates $\mathbf{r} = \mathbf{x} - \mathbf{x}'$,

$$K(\mathbf{r}) = \langle\rho(\mathbf{x})\rho(\mathbf{x} + \mathbf{r})\rangle \tag{5}$$

or by its Fourier transform, i.e., the spectral density of inhomogeneities

$$S(\mathbf{k}) = \int K(\mathbf{r})e^{-i\mathbf{k}\cdot\mathbf{r}}d\mathbf{r}. \tag{6}$$

Substituting Eq. (4) into the system of Eqs. (1) and (2), we rewrite the system in the matrix form

$$[\hat{L}(\mathbf{x}) - \hat{R}(\mathbf{x})]\hat{Z}(\mathbf{x}) = \hat{F}(\mathbf{x}), \tag{7}$$

where

$$\hat{L}(\mathbf{x}) = \begin{bmatrix} \nabla^2 + \nu_m & -\dfrac{\varepsilon M}{\mu}\dfrac{\partial}{\partial z} \\ \dfrac{\varepsilon M}{\alpha}\dfrac{\partial}{\partial z} & \nabla^2 + \nu_u \end{bmatrix}, \tag{8}$$

$$\hat{R}(\mathbf{x}) = \begin{bmatrix} 0 & \dfrac{\Delta\varepsilon}{\mu}M\rho(\mathbf{x})\dfrac{\partial}{\partial z} \\ -\dfrac{\Delta\varepsilon}{\alpha}M\left(\dfrac{\partial}{\partial z}\rho(\mathbf{x}) + \rho(\mathbf{x})\dfrac{\partial}{\partial z}\right) & 0 \end{bmatrix}, \tag{9}$$

$$\hat{Z}(\mathbf{x}) = \begin{bmatrix} \alpha m \\ \mu u \end{bmatrix}, \quad \hat{F}(\mathbf{x}) = \begin{bmatrix} -h \\ -f \end{bmatrix}. \tag{10}$$

Here, it is seen that αm and μu are normalized variables for the coupled system of equations. We also use this normalization to introduce the unaveraged matrix Green's function of the system by writing the equation for it in the form

$$[\hat{L}(\mathbf{x}) - \hat{R}(\mathbf{x})] = \hat{\tilde{G}}(\mathbf{x}, \mathbf{x}_0) = \delta(\mathbf{x} - \mathbf{x}_0)\hat{E}. \tag{11}$$

Here,

$$\hat{\tilde{G}}(\mathbf{x}, \mathbf{x}_0) = \begin{bmatrix} \tilde{G}_{mm}(\mathbf{x}, \mathbf{x}_0) & \tilde{G}_{mu}(\mathbf{x}, \mathbf{x}_0) \\ \tilde{G}_{um}(\mathbf{x}, \mathbf{x}_0) & \tilde{G}_{uu}(\mathbf{x}, \mathbf{x}_0) \end{bmatrix}, \tag{12}$$

where $\tilde{G}_{mm}(\tilde{G}_{uu})$ and $\tilde{G}_{mu}$ ($\tilde{G}_{um}$) are the spin (elastic) Green's functions, respectively, at the magnetic and elastic point excitations, respectively; $\delta(\mathbf{x} - \mathbf{x}_0)$ is the Dirac delta function; and

$$\hat{E} = \begin{bmatrix} 1 & 0 \\ 0 & 1 \end{bmatrix} \tag{13}$$

is the identity matrix. To obtain the averaged Green's function $\hat{G}$, we use the new SCA [33], which for the crossing resonance has the form of a system of three coupled matrix equations [35]: the Dyson equation for the averaged matrix Green's function $\hat{G}$,

$$\begin{aligned}\hat{G}(\mathbf{x}, \mathbf{x}_0) = \hat{g}(\mathbf{x}, \mathbf{x}_0) + \iint \hat{G}(\mathbf{x}, \mathbf{x}')\hat{E}_1(\mathbf{x}') \\ \times \hat{\Sigma}(\mathbf{x}', \mathbf{x}'')\hat{E}_1(\mathbf{x}'')\hat{g}(\mathbf{x}'', \mathbf{x}_0)d\mathbf{x}'\,d\mathbf{x}'',\end{aligned} \tag{14}$$

the equation for the self-energy matrix $\hat{\Sigma}$,

$$\hat{\Sigma}(\mathbf{x}',\mathbf{x}'') = \gamma^2 \iint K(\mathbf{x}_2,\mathbf{x}'')\hat{\Gamma}(\mathbf{x}',\mathbf{x}_1;\mathbf{x}_2) \times \hat{J}\hat{X}(\mathbf{x}_1,\mathbf{x}'')\hat{J}d\mathbf{x}_1 d\mathbf{x}_2 \quad (15)$$

and the equation for the matrix vortex function $\hat{\Gamma}$,

$$\hat{\Gamma}(\mathbf{x}',\mathbf{x}_1;\mathbf{x}_2) \approx \delta(\mathbf{x}'-\mathbf{x}_2)\delta(\mathbf{x}'-\mathbf{x}_1)\hat{E} + \gamma^2 \iiint K(\mathbf{x}_1,\mathbf{x}_4)\hat{\Gamma}(\mathbf{x}',\mathbf{x}_3;\mathbf{x}_4)\hat{J}\hat{X}(\mathbf{x}_3,\mathbf{x}_5) \times \hat{\Gamma}(\mathbf{x}_5,\mathbf{x}_6;\mathbf{x}_2)\hat{J}\hat{X}(\mathbf{x}_6,\mathbf{x}_1)d\mathbf{x}_3 d\mathbf{x}_4 d\mathbf{x}_5 d\mathbf{x}_6, \quad (16)$$

Here, $K(\mathbf{x}_1, \mathbf{x}_4)$ is the correlation function,

$$\hat{X}(\mathbf{x}_1,\mathbf{x}'') = \hat{E}_1(\mathbf{x}_1)\hat{G}(\mathbf{x}_1,\mathbf{x}'')\hat{E}_1(\mathbf{x}''), \quad \hat{J} = \begin{bmatrix} 0 & \sqrt{\alpha/\mu} \\ \sqrt{\mu/\alpha} & 0 \end{bmatrix} \quad (17)$$

and

$$\gamma = \frac{\Delta\varepsilon}{\sqrt{\alpha\mu}}M, \quad (18)$$

and $\hat{g}(\mathbf{x}, \mathbf{x}_0)$ is the Green's function of the homogeneous medium, which is a solution of the equation

$$\hat{L}(\mathbf{x})\hat{g}(\mathbf{x},\mathbf{x}_0) = \delta(\mathbf{x}-\mathbf{x}_0)\hat{E}. \quad (19)$$

The Fourier transforms of all matrix quantities

$$\hat{Y}(\mathbf{x}) = (2\pi)^{-d}\int \hat{Y}_{\mathbf{k}} e^{i\mathbf{k}\cdot\mathbf{x}}d\mathbf{k}, \quad (20)$$

$$\hat{Y}_{\mathbf{k}} = \int \hat{Y}(\mathbf{x})e^{-i\mathbf{k}\cdot\mathbf{x}}d\mathbf{x}, \quad (21)$$

where d is the dimensionality of the space, give the system of two coupled self-consistent equations for the matrix Green's functions $\hat{G}$ and vortex function $\hat{\Gamma}$, which is similar in structure to the system of equations of the new SCA for one wavefield [33]:

$$\hat{G}_{\mathbf{k}} = \frac{\hat{E}}{\hat{g}_{\mathbf{k}}^{-1} - \gamma^2(2\pi)^{-d}\hat{E}_{\mathbf{k}}^{(1)}\int S_{\mathbf{k}-\mathbf{k}_1}\hat{J}\hat{X}_{\mathbf{k}_1}\hat{\Gamma}_{\mathbf{k}_1,\mathbf{k}-\mathbf{k}_1}\hat{J}\hat{E}_{\mathbf{k}}^{(2)}d\mathbf{k}_1}, \quad (22)$$

$$\hat{\Gamma}_{\mathbf{k}_1,\mathbf{k}-\mathbf{k}_1} \approx \frac{\hat{E}}{\hat{E} - \gamma^2(2\pi)^{-d}\int S_{\mathbf{k}_1-\mathbf{k}_2}\hat{\Gamma}_{\mathbf{k}_2,\mathbf{k}_1-\mathbf{k}_2}\hat{J}\hat{X}_{\mathbf{k}_2}\hat{J}\hat{X}_{\mathbf{k}-\mathbf{k}_1+\mathbf{k}_2}d\mathbf{k}_2}. \quad (23)$$

Here,

$$\hat{X}_{\mathbf{k}_1} = \hat{E}_{\mathbf{k}_1}^{(2)}\hat{G}_{\mathbf{k}_1}\hat{E}_{\mathbf{k}_1}^{(1)}, \quad (24)$$

$$\hat{g}_{\mathbf{k}}^{-1} = \begin{bmatrix} \nu_m - k^2 & -i(\varepsilon/\mu)Mk_z \\ i(\varepsilon/\alpha)Mk_z & \nu_u - k^2 \end{bmatrix}, \quad \hat{g}_{\mathbf{k}} = \begin{bmatrix} g_{mm}(\mathbf{k}) & ig_{mu}(\mathbf{k}) \\ -ig_{um}(\mathbf{k}) & g_{uu}(\mathbf{k}) \end{bmatrix}, \quad (25)$$

$$\hat{E}_{\mathbf{k}}^{(1)} = \begin{bmatrix} 1 & 0 \\ 0 & -ik_z \end{bmatrix}, \quad \hat{E}_{\mathbf{k}}^{(2)} = \begin{bmatrix} 1 & 0 \\ 0 & ik_z \end{bmatrix}. \quad (26)$$

Similar to the initial matrix Green's function $\hat{G}_{\mathbf{k}}$, we represent the matrix Green's function $\hat{g}_{\mathbf{k}}$ in the form

$$\hat{G}_{\mathbf{k}} = \begin{bmatrix} G_{mm}(\mathbf{k}) & iG_{mu}(\mathbf{k}) \\ -iG_{um}(\mathbf{k}) & G_{uu}(\mathbf{k}) \end{bmatrix}. \quad (27)$$

The elements of the initial matrix Green's function $\hat{g}_{\mathbf{k}}$ have the form

$$g_{mm}(\mathbf{k}) = \frac{\nu_u - k^2}{(\nu_m - k^2)(\nu_u - k^2) - \gamma_0^2 k_z^2}, \quad g_{mu}(\mathbf{k}) = \frac{(\varepsilon/\mu)Mk_z}{(\nu_m - k^2)(\nu_u - k^2) - \gamma_0^2 k_z^2}, \quad g_{um}(\mathbf{k}) = \frac{(\varepsilon/\alpha)Mk_z}{(\nu_m - k^2)(\nu_u - k^2) - \gamma_0^2 k_z^2}, \quad g_{uu}(\mathbf{k}) = \frac{\nu_m - k^2}{(\nu_m - k^2)(\nu_u - k^2) - \gamma_0^2 k_z^2}, \quad (28)$$

where

$$\gamma_0 = \frac{\varepsilon}{\sqrt{\alpha\mu}}M. \quad (29)$$

The amplitudes m and u are expressed in terms of the averaged Green's functions as

$$m(\mathbf{k}) = -\frac{1}{\alpha}[G_{mm}(\mathbf{k})h(\mathbf{k}) + iG_{mu}(\mathbf{k})f(\mathbf{k})], \quad (30)$$

$$u(\mathbf{k}) = -\frac{1}{\mu}[G_{uu}(\mathbf{k})f(\mathbf{k}) - iG_{um}(\mathbf{k})h(\mathbf{k})]. \quad (31)$$

2.2. Analysis of the Elements of the Matrix Green's function

Below, we consider only one-dimensional inhomogeneities of the coupling parameter $\varepsilon(\mathbf{x}) = \varepsilon(x)$. In this case, $d = 1$ in Eqs. (20)–(31) and the vector $\mathbf{k}$ has only one component $k_x = k$. The correlation properties of the random function $\rho(x)$ are simulated by an exponential correlation function

$$K(r) = \exp(-k_c|x - x'|), \quad S_k = \frac{2k_c}{k_c^2 + k^2}, \quad (32)$$

where $r = |x - x'|$ and k_c is the correlation wavenumber of inhomogeneities ($r_c = k_c^{-1}$ is the correlation radius of inhomogeneities).

To analyze the fine structure at both crossing points of dispersion curves of spin and elastic waves, we consider the matrix Green's function in the case of the complete stochastization of the coupling parameter ($\varepsilon = 0$ and $\Delta\varepsilon \neq 0$), where the fine structure is most pronounced. Then, the system of Eqs. (22)–(28) is simplified: all off-diagonal elements vanish because $G_{mu}(k) = G_{um}(k) \propto \varepsilon$, and the initial Green's functions

$\hat{g}_{\mathbf{k}}$ are expressed in an explicit form. For the numerical analysis, it is convenient to represent the diagonal elements for spin and elastic waves in the form of recurrence formulas

$$G_{mm}^{(n)}(k) = \left[g_{mm}^{-1}(k) - \gamma^2 \frac{1}{2\pi} \int k_1^2 S(k-k_1) \times G_{uu}^{(n-1)}(k_1) \Gamma_{mm}^{(m)}(k_1, k-k_1) dk_1 \right]^{-1}, \quad (33)$$

$$G_{uu}^{(n)}(k) = \left[g_{uu}^{-1}(k) - \gamma^2 k^2 \frac{1}{2\pi} \int S(k-k_1) \times G_{mm}^{(n-1)}(k_1) \Gamma_{uu}^{(m)}(k_1, k-k_1) dk_1 \right]^{-1}, \quad (34)$$

respectively. Here,

$$\Gamma_{mm}^{(m)}(k_1, k-k_1) \approx \left[1 - \gamma^2 \frac{1}{2\pi} \int (k-k_1+k_2)^2 \times S(k_1-k_2) \Gamma_{mm}^{(m-1)}(k_2, k_1-k_2) G_{mm}^{(n)}(k_2) \times G_{uu}^{(n)}(k-k_1+k_2) dk_2 \right]^{-1}, \quad (35)$$

$$\Gamma_{uu}^{(m)}(k_1, k-k_1) \approx \left[1 - \gamma^2 \frac{1}{2\pi} \int k_2^2 S(k_1-k_2) \times \Gamma_{uu}^{(m-1)}(k_2, k_1-k_2) G_{uu}^{(n)}(k_2) G_{mm}^{(n)}(k-k_1+k_2) dk_2 \right]^{-1}, \quad (36)$$

$$g_{mm}(k) = \frac{1}{\nu_m - k^2}, \quad g_{uu}(k) = \frac{1}{\nu_u - k^2}, \quad (37)$$

and the superscripts n and m indicate the iteration numbers for the Green's and vortex functions, respectively.

The first approximation of Eqs. (33)–(36) is obtained by substituting $\Gamma_{mm}^{(0)} = 1$, $\Gamma_{uu}^{(0)} = 1$, $G_{mm}^{(0)} = g_{mm}$, $G_{uu}^{(0)} = g_{uu}$ into the integrands:

$$G_{mm}^{(1)}(k) = \left[g_{mm}^{-1}(k) - \frac{\gamma^2}{2\pi} \int k_1^2 S(k-k_1) g_{uu}(k_1) dk_1 \right]^{-1}, \quad (38)$$

$$G_{uu}^{(1)}(k) = \left[g_{uu}^{-1}(k) - \frac{\gamma^2 k^2}{2\pi} \int S(k-k_1) g_{mm}(k_1) dk_1 \right]^{-1}, \quad (39)$$

$$\Gamma_{mm}^{(1)}(k_1, k-k_1) \approx \left[1 - \frac{\gamma^2}{2\pi} \int (k-k_1+k_2)^2 S(k_1-k_2) \times g_{mm}(k_2) g_{uu}(k-k_1+k_2) dk_2 \right]^{-1}, \quad (40)$$

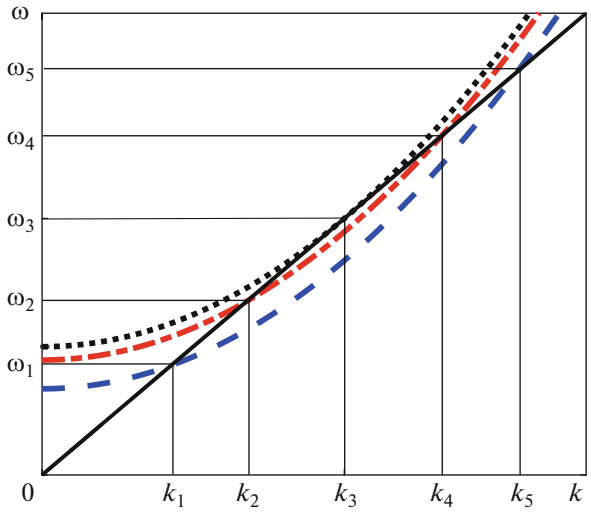

Fig. 1. (Color online) Dispersion laws of (straight line) elastic waves and (three parabolas) spin waves at three frequencies ω_0 of the uniform ferromagnetic resonance. The dispersion curves cross each other at the points (ω_n, k_n) $(n = 1, 2, 4, 5)$ and touch each other at the point (ω_3, k_3).

$$\Gamma_{uu}^{(1)}(k_1, k-k_1) \approx \left[1 - \frac{\gamma^2}{2\pi} \int k_2^2 S(k_1-k_2) \times g_{uu}(k_2) g_{mm}(k-k_1+k_2) dk_2 \right]^{-1}. \quad (41)$$

After the substitution of Eq. (32) for $S(k)$, integrals can be calculated by residues or numerically with the addition of an infinitesimal value $i\delta$ to the frequency in order to avoid divergences in the integrals. In this case, for the relaxation of waves to be due to scattering by inhomogeneities of the coupling parameter rather than to this artificial addition, the inequalities $\delta \ll v_u k_c$ and $\delta \ll v_m k_c$, where $v_m = 2gM\alpha k$ is the velocity of spin waves, should be satisfied. We substitute Eqs. (38)–(41) into Eqs. (33)–(36), perform numerical integration, and continue iterative substitutions and numerical integrations in the system of Eqs. (33)–(36) until a convergent result.

Figure 1 shows the dispersion curves of spin and elastic waves obtained neglecting the interaction between wavefields for (straight line) elastic waves,

$$\omega = v_u k, \quad (42)$$

and (three parabolas) spin waves at three frequencies ω_0 of the uniform ferromagnetic resonance,

$$\omega = \omega_0^{(l)} + \alpha g M k^2. \quad (43)$$

Here, $l = 1, 2, 3$ and $\omega_0^{(1)} < \omega_0^{(2)} < \omega_0^{(3)}$ correspond to the blue dashed, red dash-dotted, and black dotted lines, respectively. The dispersion curves cross each other at

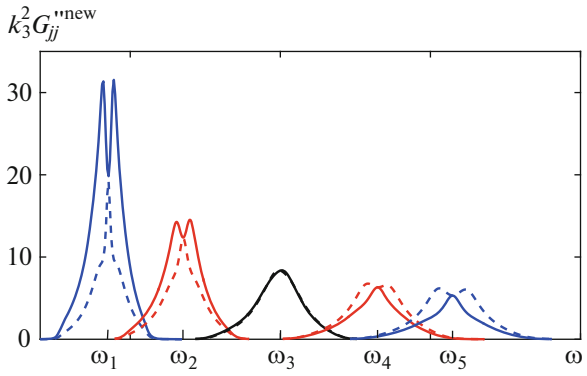

Fig. 2. (Color online) Imaginary parts (dashed curves) $G_{mm}^{"new}(\omega)$ and (solid curves) $G_{uu}^{"new}(\omega)$ of the Green's functions of spin and elastic waves, respectively, calculated in the new SCA at $k_c/k_3 = 0.01$ near the crossing frequencies ω_1, ω_2, ω_4, and ω_5 and touching frequency ω_3 of the dispersion curves.

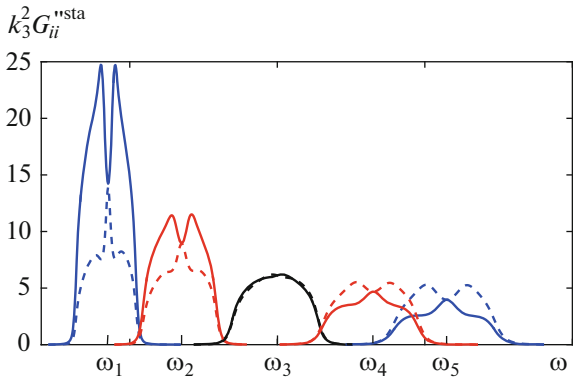

Fig. 3. (Color online) Imaginary parts (dashed curves) $G_{mm}^{"sta}(\omega, k)$ and (solid curves) $G_{uu}^{"sta}(\omega, k)$ of the Green's functions of spin and elastic waves, respectively, calculated in the standard SCA at $k_c/k_3 = 0.01$ near the crossing frequencies ω_1, ω_2, ω_4, and ω_5 and touching frequency ω_3 of the dispersion curves.

the points (ω_n, k_n) $(n = 1, 2, 4, 5)$ and touch each other at the point (ω_3, k_3).

The diagonal elements of the averaged Green's function numerically calculated by Eqs. (33) and (34) can be represented in the form of the sum of the real, G', and imaginary, $G"$, parts:

$$G_{jj}(k) = G'_{jj}(k) + iG"_{jj}(k),$$

where j takes values m or u. Figure 2 shows the frequency dependences of the imaginary parts of the Green's functions for all ω_n and k_n values. The calculation was performed at the correlation wavenumber of inhomogeneities k_c much lower than the wavenumbers k_n. With increasing n, peaks at each crossing point of curves are broadened and their amplitude decreases. The velocity of propagation of elastic waves at the first two crossing points of the curves $n = 1$ and 2 is higher than the velocity of propagation of spin waves. In Fig. 2, this is manifested as a fine structure in the form of a narrow dip at the tops of the imaginary parts of the Green's functions of elastic waves and a narrow peak at the tops of the imaginary parts of the Green's functions of spin waves. Oppositely, the velocity of spin waves at the last two points $n = 4$ and 5 is higher than the velocity of elastic waves and, correspondingly, the fine structure has the form opposite to the structure at the points $n = 1$ and 2. Here, a narrow dip is observed on the tops of the imaginary parts of the Green's functions of spin waves, whereas a narrow peak occurs on the tops of the imaginary parts of the Green's functions of elastic waves. The velocities of elastic and spin waves at the point of contact of dispersion curves, $n = 3$, are the same, and the fine structure of the spectrum is absent. The amplitude of the fine structure on the tops of the imaginary parts of the Green's functions depends on the ratio of the velocities of interacting waves: the higher this ratio, the more pronounced the narrow resonance and antiresonance.

Figure 3 shows the same frequency dependences of the imaginary parts of the Green's functions as in Fig. 2, but they were calculated in the cruder standard SCA. In this approximation, $\Gamma_{mm}(k_1, k - k_1) = 1$ and $\Gamma_{uu}(k_1, k - k_1) = 1$ are substituted into Eqs. (33) and (34), Eqs. (35) and (36) are omitted, and Eqs. (33) and (34) thus simplified become a complete system of self-consistent equations. Figure 3 demonstrates how the well-known defect of the standard SCA—dome-like shape of resonance peaks—distorts the more realistic picture obtained in the new SCA and shown in Fig. 2. However, the dependence of the fine structure on the ratio of velocities of interacting waves has qualitatively the same character in both the standard and new SCAs.

We now discuss the possibility and conditions for the observation of effects calculated in this section. According to the general expression (30), the calculated high-frequency susceptibility $\chi_g(\omega, k)$ is determined by the Green's function:

$$\chi_g(\omega, k_r) = \frac{m(\omega, k_r)}{h} = -\frac{G(\omega, k_r)}{\alpha}. \qquad (44)$$

The calculation was performed for the unlimited space at a fixed wavenumber $k = k_r$, where k_r corresponds to the magnetoelastic resonance. The frequency dependence of χ_g is continuous and monotonically decreasing in the entire frequency range except for a narrow vicinity of the frequency ω_r of the magnetoelastic resonance; only this vicinity is of interest for us.

The direct observation of effects of the magnetoelastic resonance can be provided by the experimental study of the shape of the high-frequency susceptibility of the spin-wave resonance in thin magnetic films.

However, the shape of the experimentally observed high-frequency susceptibility $\chi_m(\omega, k)$ significantly differs from the calculated susceptibility $\chi_g(\omega, k)$ in the unlimited space. The finiteness of the film results in the discreteness of the spectrum of spin waves $\omega_p(k_p)$ and, correspondingly, in the discrete peaks of the susceptibility $\chi_m(\omega_p, k_p)$ at $\omega = \omega_p$ in the absence of damping. Because of the broadening of spin-wave resonance lines due to damping or stochastic distribution of frequencies caused by inhomogeneities, the observed frequency dependence of χ_m is continuous and has maxima at $\omega = \omega_p$. For the appearance of effects of the magnetoelastic resonance, the wavenumber k_p of one of these resonances should be equal to the wavenumber k_r:

$$k_r = k_p = \pi p/d, \tag{45}$$

where d is the thickness of the film and $p = 1, 2, 3, \ldots$. This condition can be ensured by choosing the thickness of the film. It is also necessary to take into account that the experimental measurement of $\chi_m(\omega_p, z)$ is accompanied by the self-averaging of the response over the thickness of the film:

$$\langle m_p \rangle = \frac{1}{d}\int\limits_{-d/2}^{d/2} m(\omega_p, z)dz. \tag{46}$$

Thus, because of the difference between the calculation models and observation conditions (unlimited space and thin film), only a qualitative agreement between the calculated, $\chi_g(\omega, k_r)$, and observed, $\chi_m(\omega, k_r)$, high-frequency susceptibilities can be expected. However, all features of the fine structure of the magnetoelastic resonance calculated for $\chi_g(\omega, k_r)$ will be manifested in $\chi_m(\omega, k_r)$ if the damping-induced broadening of spin-wave resonance lines is much smaller than broadening caused by the stochastic frequency distribution.

3. MODEL OF ORIGIN OF THE FINE STRUCTURE IN THE SPECTRUM OF THE CROSSING RESONANCE

To demonstrate the origin of the fine structure of the crossing resonance spectrum in the medium with an inhomogeneous coupling parameter, we use a simple model with the infinite correlation radius ($k_c = 0$, the model of independent crystallites), which is described by Eqs. (63) in [35].

In this case, the random functions $\rho(\mathbf{x})$ are transformed to random values ρ whose stochastic properties are described by a certain distribution function $f(\rho)$, which can generally be arbitrary. The elements of the matrix Green's function depending on ρ in the case of the complete stochastization of the coupling parameter ($\varepsilon = 0$ and $\Delta\varepsilon \neq 0$) have the form

$$\tilde{G}_{mm}(\omega, k; \rho) = \frac{\nu_u - k^2}{(\nu_m - k^2)(\nu_u - k^2) - (\gamma\rho k)^2}, \tag{47}$$

$$\tilde{G}_{uu}(\omega, k; \rho) = \frac{\nu_m - k^2}{(\nu_m - k^2)(\nu_u - k^2) - (\gamma\rho k)^2}. \tag{48}$$

The averaged Green's functions are given by the expressions

$$\check{G}_{mm}(\omega, k) = \int \tilde{G}_{mm}(\omega, k; \rho) f(\rho) d\rho, \tag{49}$$

$$\check{G}_{uu}(\omega, k) = \int \tilde{G}_{uu}(\omega, k; \rho) f(\rho) d\rho. \tag{50}$$

Here, we supplement this model by introducing the phenomenological damping parameter Γ_m and Γ_u of spin and elastic waves, respectively. We consider frequencies near the magnetoelastic resonance frequency ω_r at the wavenumber $k = k_r$. For this reason, we analyze only one branch of the dispersion curve of elastic waves and represent the diagonal Green's functions of coupled spin and elastic waves in the form

$$\tilde{G}_{mm}(\omega) = \frac{\omega - \omega_u - i\Gamma_u}{(\omega - \omega_m - i\Gamma_m)(\omega - \omega_u - i\Gamma_u) - \eta^2}, \tag{51}$$

$$\tilde{G}_{uu}(\omega) = \frac{\omega - \omega_m - i\Gamma_m}{(\omega - \omega_m - i\Gamma_m)(\omega - \omega_u - i\Gamma_u) - \eta^2}, \tag{52}$$

where

$$\omega_m = \omega_0 + \omega_M \alpha k^2, \tag{53}$$

$$\omega_u = v_u k, \tag{54}$$

$$\eta \approx \Delta\varepsilon M \sqrt{\frac{\omega_M \omega_u}{2\mu}}\rho. \tag{55}$$

We consider Eqs. (51) and (52) at $k = k_r$, when $\omega_m = \omega_u = \omega_r$:

$$\tilde{G}_{mm}(\kappa) = \frac{\zeta - i\Gamma_u}{(\zeta - i\Gamma_m)(\zeta - i\Gamma_u) - \eta^2}, \tag{56}$$

$$\tilde{G}_{uu}(\kappa) = \frac{\zeta - i\Gamma_m}{(\zeta - i\Gamma_m)(\zeta - i\Gamma_u) - \eta^2}, \tag{57}$$

where $\zeta = \omega - \omega_r$. The real and imaginary parts of the eigenfrequencies as functions of the coupling parameter η are obtained from the condition of zero denominator of the right-hand sides of Eqs. (56) and (57):

$$\omega'_{\pm} = \begin{cases} \omega_r, & \eta < \eta_c, \\ \omega_r \pm \sqrt{\eta^2 - \eta_c^2}, & \eta > \eta_c, \end{cases} \tag{58}$$

$$\omega''_{\pm} = \begin{cases} \Gamma \pm \sqrt{\eta^2 - \eta_c^2}, & \eta < \eta_c, \\ \Gamma, & \eta > \eta_c, \end{cases} \tag{59}$$

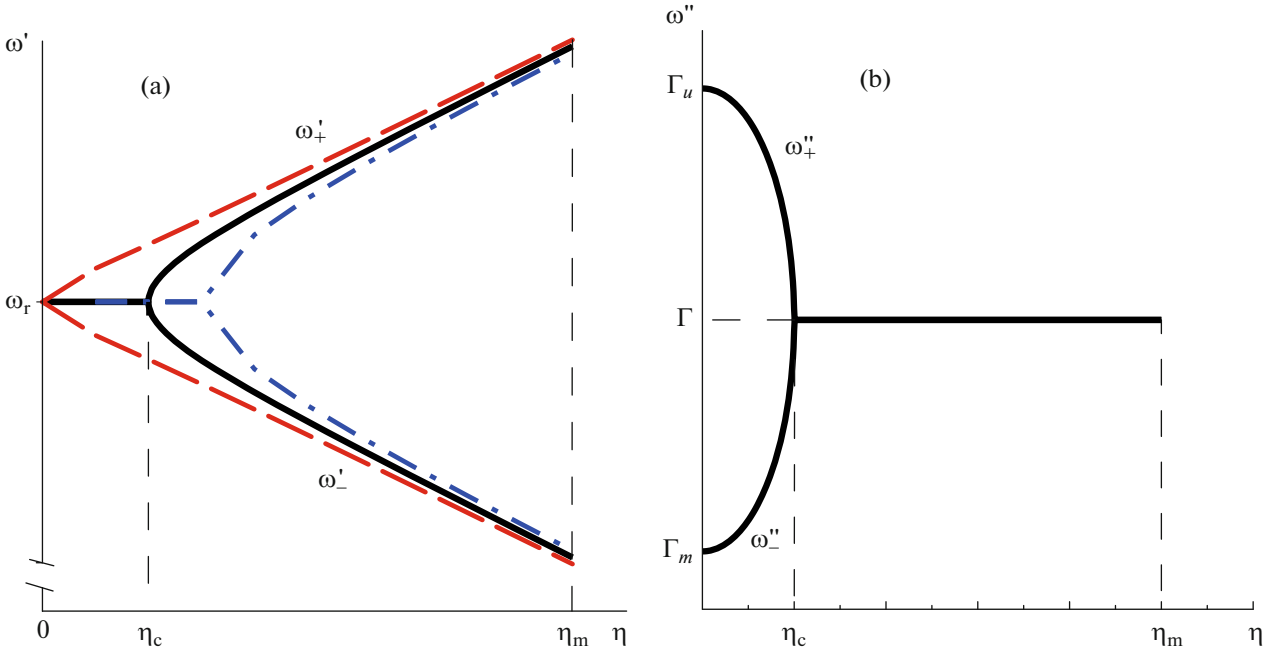

Fig. 4. (Color online) (a) (Black solid curve) Real part of the frequency and (red dashed and blue dash-dotted curves) positions of the maxima of the imaginary parts of the Green's functions $\tilde{G}''_{uu}$ and $\tilde{G}''_{mm}$, respectively, and (b) the imaginary part of the frequency versus the coupling parameter η. The critical value $\eta = \eta_c$ separates the degenerate and nondegenerate parts of the spectrum.

where

$$\eta_c = \frac{1}{2}|\Gamma_u - \Gamma_m|, \tag{60}$$

$$\Gamma = \frac{1}{2}(\Gamma_u + \Gamma_m). \tag{61}$$

The dependences of ω' and ω'' on the coupling parameter η are shown in Fig. 4. It is seen that the removal of the degeneracy of eigenfrequencies has a threshold character in the coupling parameter η. The real parts of the frequencies remain degenerate ($\omega'_+ = \omega'_- = \omega_r$) at the variation of the coupling parameter from zero to the critical (threshold) value $\eta = \eta_c$ given by Eq. (60). Then, degeneracy is lifted and the gap $\Delta\omega = \omega'_+ - \omega'_-$ appears in the spectrum and increases with η, reaching the maximum

$$\Delta\omega = 2\sqrt{\eta_m^2 - \eta_c^2}, \tag{62}$$

at $\eta = \eta_m$, where η_m is the maximum coupling parameter in a given material. Unlike the real parts, the imaginary parts $\omega''_\pm$ of frequencies are degenerate in the η interval from η_c to η_m. The damping of the eigenfrequencies $\omega''_\pm$ in this range is the same and is determined by the half-sum of the damping parameters Γ_m and Γ_u. At $\eta < \eta_c$, the degeneracy of the imaginary parts of the frequencies is lifted: a decrease in η is accompanied by an increase in ω''_+ and a decrease in ω''_-, which reach the limiting values $\omega''_+ = \Gamma_u$ and $\omega''_- = \Gamma_m$ at $\eta = 0$. For negative coupling parameters, each of the plots in Fig. 4 has a mirror symmetry if the magnitudes of the maxima η_m are the same for $\eta > 0$ and $\eta < 0$ (the magnitudes of η_c are the same by definition, see Eq. (60)).

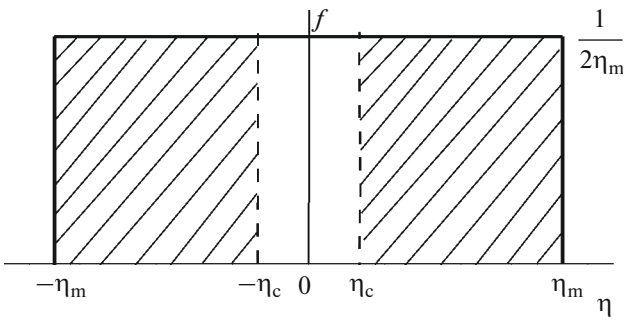

Fig. 5. Model of the distribution function $f(\eta)$.

The simplest symmetric rectangular distribution function $f(\eta)$ of random realizations of the coupling parameter at a nonzero difference between damping parameters in the system of two interacting wavefields is shown in Fig. 5. The eigenfrequencies $\omega'_\pm$ in the regions with $0 < |\eta| < |\eta_c|$ are degenerate in spite of a nonzero coupling parameter η. Degeneracy is lifted only in the shaded regions in Fig. 5 when the coupling parameter η is above the threshold value η_c. We emphasize that the appearance of unshaded sub-

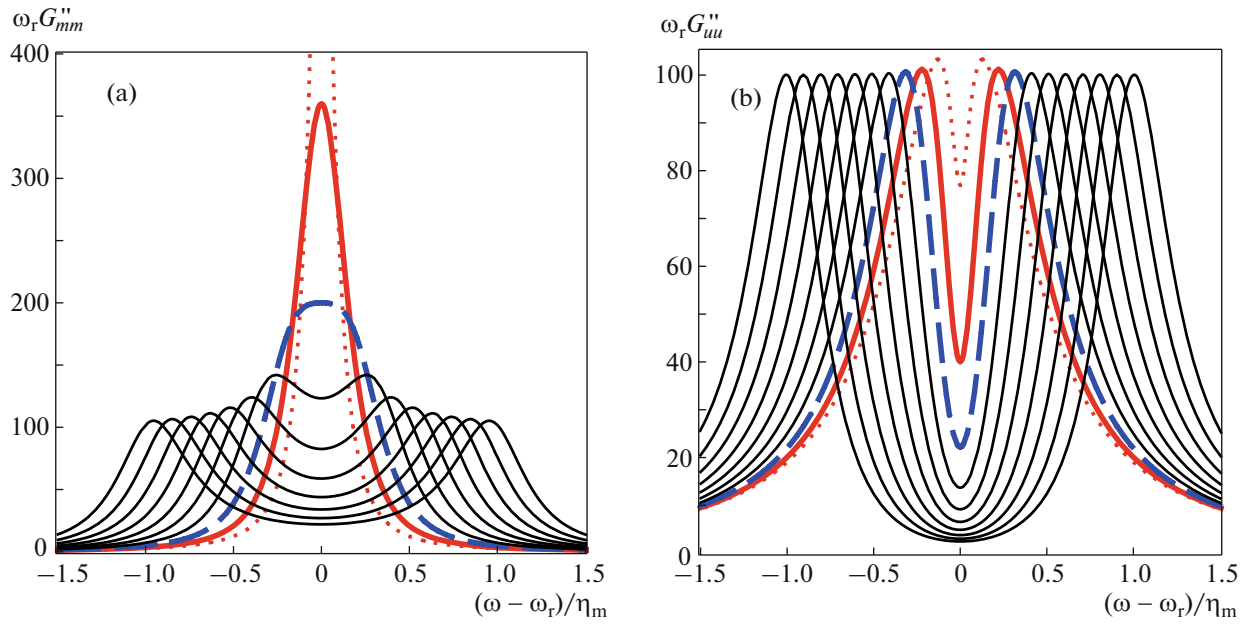

Fig. 6. (Color online) Imaginary parts of the diagonal Green's functions of (a) spin and (b) elastic waves at the point $k = k_r$ for (thin black solid lines) $\eta > 1.5\eta_c$, (blue dashed curves) $\eta = 1.5\eta_c$, (red thick solid curves) $\eta = \eta_c$, and (red dotted curves) $\eta = 0.5\eta_c$.

threshold regions is due not to damping but to the difference between the damping parameters: when $\Gamma_u = \Gamma_m$, degeneracy is lifted at any $|\eta| \neq 0$.

The imaginary parts of random realizations of the Green's functions $\tilde{G}_{mm}$ and $\tilde{G}_{uu}$ have the form

$$\tilde{G}''_{mm}(\zeta;\eta) = \frac{\Gamma_u\tilde{\eta}^2 + \zeta^2\Gamma_m}{(\zeta^2 - \tilde{\eta}^2)^2 + 4\Gamma^2\zeta^2}, \quad (63)$$

$$\tilde{G}''_{uu}(\zeta;\eta) = \frac{\Gamma_m\tilde{\eta}^2 + \zeta^2\Gamma_u}{(\zeta^2 - \tilde{\eta}^2)^2 + 4\Gamma^2\zeta^2}, \quad (64)$$

where

$$\tilde{\eta}^2 = \eta^2 + \Gamma_u\Gamma_m. \quad (65)$$

The functions $\tilde{G}''_{mm}(\zeta)$ and $\tilde{G}''_{uu}(\zeta)$ at several η values are shown in Fig. 6. A series of curves at various values $\eta > 1.5\eta_c$ corresponds to the shaded regions in Fig. 5 where degeneracy is lifted. Here, each curve has the usual two maxima at $\zeta_{1,2} \approx \pm\tilde{\eta}$. The functions $\tilde{G}''_{mm}(\zeta)$ and $\tilde{G}''_{uu}(\zeta)$ at these maxima are approximately the same:

$$\tilde{G}''_{uu}(\zeta)|_{\zeta^2=\tilde{\eta}^2} \approx \tilde{G}''_{mm}(\zeta)|_{\zeta^2=\tilde{\eta}^2} \approx \frac{1}{2\Gamma}. \quad (66)$$

As η decreases and approaches the critical value η_c, the difference between the functions $\tilde{G}''_{mm}(\zeta)$ and $\tilde{G}''_{uu}(\zeta)$ appears. At $\eta < 1.5\eta_c$, the function $\tilde{G}''_{mm}(\zeta)$ has one peak, whereas the function $\tilde{G}''_{uu}(\zeta)$ has two peaks (blue dashed lines). Differences between these functions are particularly large in the region $\eta \leq \eta_c$ corresponding to the degeneracy of the oscillation frequencies. Expressions (63) and (64) at $\zeta = \eta_c$ are simplified to the form

$$\tilde{G}''_{mm}(\zeta) = \frac{\zeta^2\Gamma_m + \Gamma_u\Gamma^2}{(\zeta^2 + \Gamma^2)^2}, \quad (67)$$

$$\tilde{G}''_{uu}(\zeta) = \frac{\zeta^2\Gamma_u + \Gamma_m\Gamma^2}{(\zeta^2 + \Gamma^2)^2}. \quad (68)$$

These expressions correspond to red thick solid lines in Fig. 6. Both Eqs. (67) and (68) have the same mathematical form. The denominator corresponds to a single resonance maximum at the point $\zeta = 0$, whereas the numerator corresponds to the resonance minimum at the same point. The characteristics of the resonance maximum are identical for both functions $\tilde{G}''_{mm}(\zeta)$ and $\tilde{G}''_{uu}(\zeta)$, whereas the characteristics of the resonance minima are strongly different at different relations between Γ_u and Γ_m. If $\Gamma_u > \Gamma_m$ as in our case, the numerator of the function $\tilde{G}''_{mm}(\zeta)$ has a shallow broad minimum, which is suppressed by the sharp maximum of the denominator. When the derivative of the function $\tilde{G}''_{mm}(\zeta)$ is zero, one maximum should be observed at $\omega = \omega_r$. In this case, the numerator of the function $\tilde{G}''_{uu}(\zeta)$ has a narrow sharp minimum at $\omega = \omega_r$, which is manifested against the background of a broader maximum. As a result, two maxima on this function should be observed in the case $\Gamma_u > 2\Gamma_m$ at the frequencies

$$\omega_\pm = \omega_r \pm \Gamma\sqrt{1 - \frac{2\Gamma_m}{\Gamma_u}}. \quad (69)$$

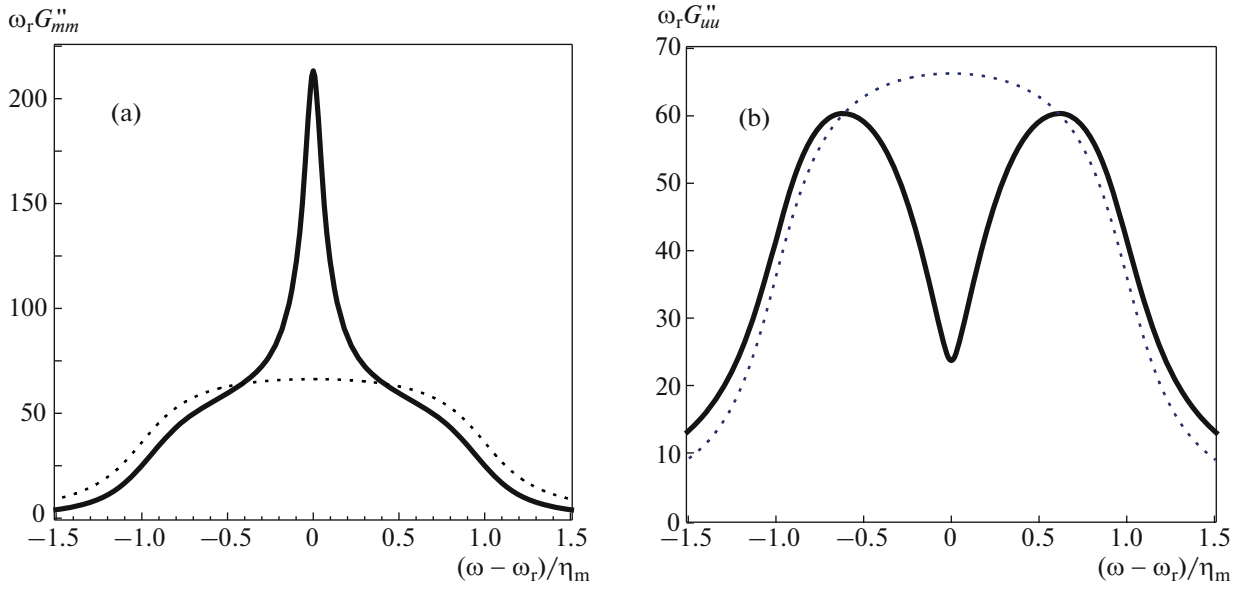

Fig. 7. Averaged imaginary parts of the diagonal Green's functions of the (a) spin and (b) elastic waves at the point $k = k_r$ for (solid curves) $\Gamma_m \neq \Gamma_u$ and (dotted curves) $\Gamma_m = \Gamma_u$ ($\eta_c = 0$).

The red thick line in Fig. 6b corresponding to this situation is similar to neighboring thin lines corresponding to the degeneracy removal region. However, according to Eq. (69), the splitting of the maximum on this line into two peaks does not mean the appearance of a gap in the spectrum. Intervals between these maxima decrease with a further decrease in η (Fig. 6b, red dotted line). The dependence of the interval between the peaks on η is shown in Fig. 4a (red dashed line). Figure 4a also shows the dependence of the positions of the maxima of the function $\tilde{G}''_{mm}(\zeta)$ on η (blue dash-dotted line). It is seen that the dependence of the position of the maxima of the Green's functions $\tilde{G}''_{mm}(\zeta)$ and $\tilde{G}''_{uu}(\zeta)$ on η is significantly different from the dependence of the eigenfrequencies on η.

Random realizations in Fig. 6 can be considered as the Green's functions of homogeneous samples with the corresponding coupling parameters η. In this case, both Green's functions $\tilde{G}''_{mm}$ and $\tilde{G}''_{uu}$ of the sample with $\eta > \eta_c$ have the same form standard for crossing resonances (one of thin black lines in Figs. 6a and 6b), whereas the forms of the functions $\tilde{G}''_{mm}$ and $\tilde{G}''_{uu}$ for the sample with $\eta < \eta_c$ are different and correspond to resonance and antiresonance (red lines in Figs. 6a and 6b, respectively) of the fine structure of the spectrum, respectively.

Both situations corresponding to the nondegenerate and degenerate spectra of eigenfrequencies can also be observed in an appropriately oriented single crystal. The magnitude and sign of the coupling parameter η in many materials are different along different crystallographic axes [36, 37]. In particular, the parameter η in an iron single crystal is positive and negative along the [100] and [111] axes, respectively, and has intermediate values along other directions. In the situation with the oriented single crystal, as well as in the situation with materials with different η values, degenerate and nondegenerate spectra can be observed only separately.

We now average Eqs. (63) and (64) for the imaginary parts of the Green's functions over the coupling parameter η with the distribution function (see Fig. 5) by numerical integration (Fig. 7). It is seen that the plots of the averaged Green's functions $\tilde{G}''_{mm}(\zeta)$ and $\tilde{G}''_{uu}(\zeta)$ in the considered model clearly exhibit the main feature of the fine structure of the magnetoelastic resonance, i.e., the appearance of a narrow resonance on the function $\tilde{G}''_{mm}(\zeta)$ and a narrow antiresonance on the function $\tilde{G}''_{uu}(\zeta)$ at $\omega = \omega_r$ against the background of broad maxima caused by the stochastic distribution of eigenfrequencies.

Thus, we have shown that the effects of the fine structure of the magnetoelastic spectrum occurring in inhomogeneous ferromagnets are due to the contribution of random realizations corresponding to the degenerate state of the magnetoelastic system. Such states are always present in the distribution function of the coupling parameter if the critical coupling parameter η_c given by Eq. (60) is nonzero.

4. CONCLUSIONS

This work has been devoted to determining the origin of the fine structure of the crossing resonance

spectrum of two wavefields of different natures in an inhomogeneous medium, which was predicted by analytical and numerical methods in our previous works [15–18, 33–35]. To this end, we have considered the magnetoelastic resonance at both crossing points of dispersion curves of spin and elastic waves (Section 2) and the crossing resonance in the model of the inhomogeneous medium with the infinite correlation radius (Section 3). We have studied interacting wavefields in the medium with the stochastically inhomogeneous coupling parameter between them with zero mean value, where coupling between wavefields is ensured only by spatial fluctuations of this parameter. The performed study has revealed the stage of formation of the fine structure of the spectrum, beginning with the crossing resonance in the homogeneous medium.

The removal of degeneracy of the eigenfrequencies of two wavefields of different natures $m(x, t)$ and $u(x, t)$ at the crossing point of their dispersion curves, $\omega = \omega_r$, $k = k_r$, at the appearance of the coupling η between these fields in the homogeneous medium with different relaxation parameters Γ_m and Γ_u of the corresponding waves has a threshold character. This removal occurs when the parameter η exceeds the critical value $\eta_c = |\Gamma_u - \Gamma_m|/2$. The forms of the Green's functions $\tilde{G}''_{mm}$ and $\tilde{G}''_{uu}$ of the fields $m(x, t)$ and $u(x, t)$, respectively, are strongly different in media with degenerate ($\eta < \eta_c$) and nondegenerate ($\eta > \eta_c$) frequency spectra. In media with the nondegenerate spectrum ($\eta > \eta_c$), both Green's functions $\tilde{G}''_{mm}$ and $\tilde{G}''_{uu}$ have the form of two resonance peaks with the same half-width $(\Gamma_u + \Gamma_m)/2$ spaced by the interval 2η, which is standard for crossing resonances in the homogeneous sample. In media with the degenerate frequency spectrum ($\eta < \eta_c$), the Green's functions $\tilde{G}''_{mm}$ and $\tilde{G}''_{uu}$ have different forms: if $\Gamma_m < \Gamma_u$, the function $\tilde{G}''_{mm}(\zeta)$ has the form of a narrow resonance peak at the frequency $\omega = \omega_r$, whereas the function $\tilde{G}''_{uu}$ has the form of a broader resonance peak split on the top by a narrow antiresonance at the same frequency $\omega = \omega_r$.

Thus, the main features of the fine structure of the crossing resonance in the inhomogeneous medium—a narrow resonance on the function $\tilde{G}''_{mm}$ and a narrow antiresonance at the same frequency $\omega = \omega_r$ on the function $\tilde{G}''_{uu}$—are standard for the crossing resonance in the homogeneous sample where $\eta < \eta_c$. The two forms of the spectrum of the magnetoelastic resonance corresponding to $\eta < \eta_c$ and $\eta > \eta_c$ in the homogeneous sample can be observed only separately either in different samples or in a single crystal, which allows broad ranges of variation of the magnitude and sign of the parameter η at different orientations of this crystal.

The distribution function in an inhomogeneous material (e.g., in a polycrystal with different orientations of crystallites) includes regions both with $\eta < \eta_c$ and with $\eta > \eta_c$. Averaging over the regions with $\eta > \eta_c$ leads to the formation of a broad resonance line with the half-width of about $\langle\eta^2\rangle^{1/2}$ caused by the stochastic distribution of resonance frequencies. Averaging over the regions with $\eta < \eta_c$ results in the sharpening of the resonance peak on the function G''_{mm} and the antiresonance peak on the function G''_{uu} at the same frequency $\omega = \omega_r$. As a result, the following pattern of the crossing resonance in the inhomogeneous medium is formed: identical broad peaks on both functions G''_{mm} and G''_{uu} with a narrow resonance peak of the fine structure on the function G''_{mm} and a narrow resonance peak on the function G''_{uu}.

Thus, it has been shown that the fine structure of the spectrum of any crossing resonance of two wavefields of different natures in the inhomogeneous medium is due to the contribution of random realizations corresponding to degenerate eigenfrequencies of the system.

The damping parameters $\Gamma_m(k) \propto k_c v_m$ and $\Gamma_u(k) \propto k_c v_u$ of spin and elastic waves proportional to the correlation wavenumber k_c of inhomogeneities and to the velocity of the corresponding waves, which are summed with the uniform damping parameters Γ_m and Γ_u of the same waves, occur in a ferromagnet with the spatially inhomogeneous coupling parameter. This situation has been considered in this work in the new SCA for the case where the contribution of the uniform damping parameter is negligibly small. It has been shown that the form of the fine structure on the functions G''_{mm} and G''_{uu} at the second (high-frequency) crossing point of the dispersion curves of spin and elastic waves changes to the opposite form: a narrow resonance peak of the fine structure occurs on the function G''_{uu} and an antiresonance peak appears on the function G''_{mm} because $v_m < v_u$ and $v_m > v_u$ at the points of the first and second crossings, respectively. If the contribution of uniform damping parameters Γ_m and Γ_u is large, the form of the fine structure of the spectrum at both the first and second crossing points of dispersion curves is determined by the ratio of these damping parameters. In this work, we have studied the case of the complete stochastization of the coupling parameter ($\varepsilon = 0$ and $\Delta\varepsilon \neq 0$), when the fine structure is the most pronounced. As we showed in [17, 35], the fine structure is also manifested at a nonzero mean value of the coupling parameter. As far as we know, the fine structure of the spectrum of the magnetoelastic resonance has not yet been observed experimentally.

REFERENCES

1. A. I. Akhiezer, in *Proceedings of the Workshop on Physics of Magnetic Phenomena, Moscow, May 23–31, 1956* (Metallurgizdat, Sverdlovsk, 1956).
2. E. A. Turov and Yu. P. Irkhin, Fiz. Met. Metalloved. **3**, 15 (1956).
3. A. I. Akhiezer, V. G. Bar'yakhtar, and S. V. Peletminskii, Sov. Phys. JETP **8**, 157 (1958).
4. C. Kittel, Phys. Rev. **110**, 835 (1958).
5. A. I. Akhiezer, V. G. Bar'yakhtar, and M. I. Kaganov, Sov. Phys. Usp. **3**, 567 (1960).
6. A. I. Akhiezer, V. G. Bar'yakhtar, and S. V. Peletminskii, *Spin Waves* (Nauka, Moscow, 1967; North-Holland, Amsterdam, 1968).
7. V. V. Lemanov, in *Physics of Magnetic Insulators, Collection of Articles*, Ed. by G. A. Smolenskii (Nauka, Leningrad, 1975), p. 85 [in Russian].
8. O. Yu. Belyaeva, L. K. Zarembo, and S. N. Karpachev, Sov. Phys. Usp. **35**, 106 (1992).
9. V. G. Bar'yakhtar, A. G. Danilevich, and V. A. L'vov, Phys. Rev. B **84**, 134304 (2011).
10. V. A. Ignatchenko and L. I. Deich, Phys. Rev. B **50**, 16364 (1994).
11. L. I. Deich and V. A. Ignatchenko, J. Exp. Theor. Phys. **80**, 478 (1995).
12. L. I. Deich and A. A. Lisyansky, Phys. Lett. A **220**, 125 (1996).
13. V. A. Ignatchenko, M. V. Erementchouk, A. A. Maradudin, and L. I. Deich, Phys. Rev. B **59**, 9185 (1999).
14. R. C. Bourret, Nuovo Cim. **26**, 1 (1962).
15. V. A. Ignatchenko and D. S. Polukhin, Solid State Phenom. **190**, 51 (2012).
16. V. A. Ignatchenko and D. S. Polukhin, J. Exp. Theor. Phys. **116**, 206 (2013).
17. V. A. Ignatchenko and D. S. Polukhin, J. Exp. Theor. Phys. **117**, 846 (2013).
18. V. A. Ignatchenko and D. S. Polukhin, Solid State Phenom. **215**, 105 (2014).
19. A. B. Migdal, Sov. Phys. JETP **7**, 996 (1958).
20. R. H. Kraichnan, J. Math. Phys. **2**, 124 (1961).
21. H. Bruus and K. Flensberg, *Introduction to Many-Body Quantum Theory in Condensed Matter Physics* (Orsted Labor., Niels Bohr Inst., Copenhagen, Denmark, 2002).
22. M. V. Sadovskii, *Diagrammatics. Lectures on Selected Problems in Condensed Matter Theory*, 2nd ed. (Inst. Elektrofiz. UrO RAN, Ekaterinburg, 2005; World Scientific, Singapore, 2006).
23. J. Cai, X. L. Lei, and L. M. Xie, Phys. Rev. B **39**, 11618 (1989).
24. V. N. Kostur and B. Mitrovic, Phys. Rev. B **50**, 12774 (1994).
25. C. Grimaldi, L. Pietronero, and S. Strässler, Phys. Rev. Lett. **75**, 1158 (1995).
26. Y. Takada and T. Higuchi, Phys. Rev. B **52**, 12720 (1995).
27. O. V. Danylenko, O. V. Dolgov, and V. V. Losyakov, Phys. Lett. A **230**, 79 (1997).
28. G. A. Ummarino and R. S. Gonnelli, Phys. Rev. B **56**, R14279 (1997).
29. F. Cosenza, L. de Cesare, and M. Fusco Girard, Phys. Rev. B **59**, 3349 (1999).
30. O. V. Danylenko and O. V. Dolgov, Phys. Rev. B **63**, 094506 (2001).
31. J. P. Hague and N. d'Ambrumenil, J. Low Temp. Phys. **151**, 1149 (2008).
32. J. Bauer, J. E. Han, and O. Gunnarsson, Phys. Rev. B **84**, 184531 (2011).
33. V. A. Ignatchenko and D. S. Polukhin, J. Phys. A **49**, 095004 (2016).
34. V. A. Ignatchenko, D. S. Polukhin, and D. S. Tsikalov, J. Magn. Magn. Mater. **440**, 83 (2017).
35. V. A. Ignatchenko and D. S. Polukhin, J. Exp. Theor. Phys. **125**, 91 (2017).
36. K. P. Belov, *Magnetostriction Phenomena and their Technical Applications* (Nauka, Moscow, 1987) [in Russian].
37. A. P. Babichev, N. A. Babushkina, A. M. Bratkovskii, et al., *Physical Values, The Handbook*, Ed. by I. S. Grigor'ev and E. Z. Meilikhov (Energoatomizdat, Moscow, 1991) [in Russian].

Translated by R. Tyapaev